

Configuration and hindcast quality assessment of a brazilian global sub-seasonal prediction system

Article

Accepted Version

Guimarães, B. S., Coelho, C. A. S., Woolnough, S., J. ORCID: <https://orcid.org/0000-0003-0500-8514>, Kubota, P. Y., Bastarz, C. F., Figueroa, S. N., Bonatti, J. P. and Souza, D. C. (2020) Configuration and hindcast quality assessment of a brazilian global sub-seasonal prediction system. *Quarterly Journal of the Royal Meteorological Society*, 146 (728). pp. 1067-1084. ISSN 0035-9009 doi: <https://doi.org/10.1002/qj.3725> Available at <https://centaur.reading.ac.uk/88559/>

It is advisable to refer to the publisher's version if you intend to cite from the work. See [Guidance on citing](#).

To link to this article DOI: <http://dx.doi.org/10.1002/qj.3725>

Publisher: Wiley

All outputs in CentAUR are protected by Intellectual Property Rights law, including copyright law. Copyright and IPR is retained by the creators or other copyright holders. Terms and conditions for use of this material are defined in the [End User Agreement](#).

www.reading.ac.uk/centaur

CentAUR

Central Archive at the University of Reading

Reading's research outputs online

**CONFIGURATION AND HINDCAST QUALITY ASSESSMENT OF A
BRAZILIAN GLOBAL SUB-SEASONAL PREDICTION SYSTEM**

Bruno S. Guimarães^{1,2}, Caio A. S. Coelho¹, Steve J. Woolnough², Paulo Y. Kubota¹,
Carlos F. Bastarz¹, Silvio N. Figueroa¹, José P. Bonatti¹ and Dayana C. de Souza¹

1- Center for Weather Forecast and Climate Studies,

National Institute for Space Research, Cachoeira Paulista, SP, Brazil;

2- National Centre for Atmospheric Science, Department of Meteorology,

University of Reading, UK.

ABSTRACT

This paper presents the Center for Weather Forecast and Climate Studies (CPTEC) developments for configuring a global sub-seasonal prediction system and assessing its ability in producing retrospective predictions (hindcasts) for meteorological conditions of the following 4 weeks. Six Brazilian Global Atmospheric Model version 1.2 (BAM-1.2) configurations were tested in terms of vertical resolution, deep convection and boundary layer parameterizations, as well as soil moisture initialization. The aim was to identify the configuration with best performance when predicting weekly accumulate precipitation, weekly mean 2-meter temperature (T2M) and the Madden and Julian Oscillation (MJO) daily evolution. Hindcasts assessment was performed for 12 extended austral summers (November to March - 1999/2000 to 2010/2011) with two start dates for each month for the six configurations and two ensemble approaches. The first approach, referred to as Multiple Configurations Ensemble (MCEN), was formed of one ensemble member from each of the six configurations. The second, referred to as Initial Condition Ensemble (ICEN), was composed of six ensemble members produced with the chosen configuration as the best using an Empirical Orthogonal Function (EOF) perturbation methodology. The chosen configuration presented high correlation and low root mean squared error (RMSE) for precipitation and T2M anomaly predictions at the first week and these indices degraded as lead time increased, maintaining moderate performance up to week 4 over the tropical Pacific and northern South America. For MJO predictions, this configuration crossed the 0.5 bivariate correlation threshold in 18 days. The ensemble approaches improved the

24 correlation and RMSE of precipitation and T2M anomalies. ICEN improved
25 precipitation and T2M predictions performance over eastern South America at week
26 3 and over northern South America at week 4. Improvements were also noticed for
27 MJO predictions. The time to cross the above mentioned threshold increased to 21
28 days for MCEN and to 20 days for ICEN.

29 **Keywords:** MJO, Intraseasonal Variability, Forecast Verification.

30 1. INTRODUCTION

31 Forecasting for the time scale between two weeks and two months is known as sub-
32 seasonal prediction (Vitart et al., 2017). This type of forecast is a major challenge
33 because the predictability contribution from the atmospheric initial conditions is
34 reduced compared to shorter (weather) timescales, and the predictability from slowly
35 varying boundary conditions is small for 1-2 week averages, typically the focus of sub-
36 seasonal prediction, compared to seasonal timescales (Kumar et al., 2011; Lin et al.,
37 2016). The main source of predictability for sub-seasonal forecasting is the Madden -
38 Julian Oscillation (MJO) (Zhang, 2013). However, General Circulation Models (GCMs)
39 still show limitations in simulating this oscillation (Green et al., 2017; Wang et al.,
40 2018) even with important improvements achieved in recent years (Saha et al., 2014;
41 Vitart, 2014). As a consequence of these limitations, the predictive ability of GCMs in
42 the sub-seasonal scale is lower than in the weather and seasonal scales (Zhu et al.,
43 2014). For example, de Andrade et al. (2019) showed the limited predictive ability of
44 GCM for sub-seasonal precipitation predictions for lead times beyond 15 days. In
45 general, the GCMs show modest performance in specific areas such as the equatorial

46 regions of the Atlantic and Pacific oceans and over a few regions in South America at
47 this lead time.

48 In spite of these results, a tendency towards improvements in GCMs for sub-seasonal
49 predictions is seen and several meteorological centres currently operationally produce
50 this type of forecasts (Vitart, 2004; Hudson et al., 2011; Mastrangelo et al., 2012; Liu et
51 al., 2017; Weber and Mass, 2017; Liang and Lin, 2018). The Center for Weather
52 Forecast and Climate Studies [Centro de Previsão de Tempo e Estudos Climáticos
53 (CPTEC)], which plays a leading role in South America with respect to weather and
54 seasonal forecasts, is now following the trend of these meteorological centres and
55 started to develop a sub-seasonal prediction system. This is motivated by the fact that,
56 as in seasonal forecasting, South America is located in a privileged region for sub-
57 seasonal prediction, with GCMs showing better predictive ability in this region when
58 compared to other continental regions (Li and Robson, 2015; de Andrade et al., 2019).

59 The identified evolution in sub-seasonal predictions is mainly due to improvements in
60 the representation of the MJO in GCMs. For example, The European Centre for
61 Medium-Range Weather Forecasts (ECMWF) showed a mean gain of one day in MJO
62 prediction performance per year (Vitart, 2014). This indicates that in addition to
63 improvements in predictive ability for a phenomenon that manifests in the tropical
64 region, there is also associated improvement in the extratropics due to teleconnections
65 generated by the MJO (Vitart, 2017).

66 These findings are documented, in large part, thanks to the effort generated by Sub-
67 seasonal to Seasonal (S2S) Prediction Project. This project was launched jointly by the

68 World Weather Research Program (WWRP) and the World Climate Research Program
69 (WCRP) of the World Meteorological Organization (WMO) and aims to improve
70 forecast skill and understanding on the sub-seasonal to seasonal time scales and also to
71 promote its uptake by operational centres and by the applications community. Currently,
72 the S2S Prediction Project stores and disseminates near-real-time forecasts and
73 hindcasts of eleven operational and research centres for research purposes (Vitart et al.,
74 2017).

75 The Brazilian Global Atmospheric model [BAM (Figuerola et al., 2016)] is the current
76 CPTEC global atmospheric model for weather forecasting. The performance of this
77 model for sub-seasonal predictions has not been documented yet. Therefore, this study
78 presents the first outcomes of this model for sub-seasonal predictions and aims to
79 determine which model configuration presents the best performance for this time scale.
80 Special attention is given to characteristics such as vertical resolution, deep convection
81 and boundary layer parameterizations and as well as initialization of the soil moisture
82 because they have an important influence on the MJO and sub-seasonal predictions. A
83 similar approach was taken by Green et al (2017) in order to identify a model
84 configuration with best performance when producing MJO predictions. Green et al
85 (2017) evaluated the MJO predictive ability in multiphysics and multimodel global
86 ensembles, by performing two sets of hindcasts in order to test the impact of using the
87 Grell–Freitas (2014) versus the revised simplified Arakawa–Schubert (Han and Pan,
88 2011) deep convection parameterization. They revealed that the Grell–Freitas (2014)
89 convection parameterization showed better MJO prediction performance than the
90 revised simplified Arakawa–Schubert scheme.

91 The paper is organized as follows. Section 2 presents the model description, datasets
92 used for model initialization and hindcast quality assessment, the definition of the
93 experiments, ensemble approaches and the metrics used for evaluation. The
94 retrospective performance of the produced precipitation, 2-meter temperature (T2M)
95 and MJO predictions with different BAM configuration experiments, including two
96 ensemble approaches, is shown in section 3. The final section is intended for the
97 conclusion.

98 **2. MODEL DESCRIPTION, DATASETS AND EXPERIMENTAL** 99 **CONFIGURATIONS, EVALUATION METRICS AND ENSEMBLE** 100 **APPROACHES**

101 2.1. Model description

102 The model version used in this study is the current operational CPTEC global spectral
103 atmospheric model developed for numerical weather forecasting, which is known as
104 BAM version 1.2 (BAM-1.2). This model version has different options for dynamical
105 and physics parameterizations. The Eulerian advection scheme option with a two-time-
106 level Semi-Lagrangian scheme for moisture transport and microphysics prognostic
107 variables is used in this study. The physical processes of this recent operational version
108 are similar to the previous version (BAM-1.0) and are described in Figueroa et al.
109 (2016), which are: microphysics from Morrison et al. (2009), the IBIS-CPTEC surface
110 model (Kubota, 2012), the long-wave radiation scheme developed by Chou et al. (2001)
111 (CLIRAD-LW), the short-wave radiation scheme developed by Chou and Suarez (1999)
112 (CLIRAD-SW), the latter modified by Tarasova and Fomin (2000), the modified
113 Mellor-Yamada diffusion scheme for the planetary boundary layer (PBL), which is

114 based on Mellor-Yamada (1982) and is referred to as dry-PBL, and the modified Grell-
115 Dévényi deep convection scheme, which is based on Grell-Dévényi (2002). The two
116 new BAM-1.2 components are Bretherton-Park moist diffusion scheme (Bretherton and
117 Park, 2009) for the PBL, which is referred to as moist-PBL, and the revised version of
118 the simplified Arakawa-Shubert deep convection scheme (Han and Pan. 2011), which
119 were recently implemented. Following Yu et al. (2006) aerosol optical depth in the first
120 2 km of the atmosphere is specified as 0.22 over the continents and as 0.14 over the
121 oceans. The horizontal resolution used in this study is triangular truncation at 126 waves
122 (TQ126, corresponding to a grid of approximately 1.0° in latitude and longitude) and
123 two vertical resolutions are examined: 42 (L42) and 64 (L64) sigma vertical levels.

124 One of the objectives of this study is to investigate the performance of the two PBL and
125 deep convection schemes mentioned above for sub-seasonal predictions. The main
126 difference of the newly implemented moist-PBL Bretherton-Park scheme compared to
127 the dry-PBL modified Mellor-Yamada diffusion scheme is the use of moist-conserved
128 variables and an explicit entrainment closure for convective layers. Regarding the
129 convection schemes, the revised simplified Arakawa-Shubert and the previously
130 implemented modified Grell-Dévényi deep convection parameterization schemes were
131 both derived from Grell (1993), in which the cloud spectrum of the original Arakawa-
132 Schubert (1974) scheme is reduced to a single cloud using a single mass flux closure.
133 The main differences between these convection schemes implemented in BAM-1.2 are
134 the fractional entrainment rate and convection trigger formulations [see Han and Pan
135 (2011) and Figueroa et al., (2016) for additional information].

136 2.2. Datasets and experimental configurations

137 Sub-seasonal hindcasts were performed over the period defined as the extended austral
138 summer (from November to March) over the 1999/2000-2010/2011 period. Two
139 hindcasts for two selected start dates were produced for each month of a given year.
140 Starts dates vary from one month to the next and are presented in Table 1. Each hindcast
141 was run for the following 35 days after the start date (35 days of lead time). For the
142 production of these hindcasts, BAM-1.2 was not coupled with an ocean model. Instead,
143 the total Sea Surface Temperature (SST) field (not the anomaly) of each start date was
144 kept constant during the 35 days of integration (persisted SST). It is worth highlighting
145 that coupled ocean-atmosphere processes are recognized as being important on these
146 timescales (Reichler and Roads, 2005; Chen et al., 2010, Kumar et al., 2011; Shelly et
147 al., 2014), but a number of centres contributing to the S2S database [e.g., Japan
148 Meteorological Agency (JMA) and Environment and Climate Change Canada (ECCC)]
149 produce operational sub-seasonal forecasts using un-coupled systems (Vitart et al.,
150 2017). The CPTEC couple ocean-atmosphere model version which uses BAM-1.2 as
151 atmospheric component is under development. The sub-seasonal hindcast quality
152 assessment of this coupled model version will be reported in future work.

153 ERA-Interim reanalyses (Dee et al., 2011) produced by ECMWF were used in two
154 ways. Firstly, the reanalyses were used as atmospheric initial conditions for the
155 hindcasts produced with BAM-1.2. The variables required for initialization are zonal
156 and meridional wind, specific humidity, virtual temperature and ozone in 35 vertical
157 levels between 1000 hPa and 50 hPa, surface pressure and SST. The horizontal
158 resolution chosen for initialization was $1.5^{\circ} \times 1.5^{\circ}$ degrees in latitude and longitude,
159 which was interpolated to the model spectral resolution (TQ126L42, ~100km).

160 Secondly, ERA-Interim data were used as reference to assess the quality of the
161 produced hindcasts. The variables selected for this assessment are T2M and zonal and
162 meridional winds at 850 hPa and 200 hPa.

163 To assess precipitation hindcasts quality, daily data from the Global Precipitation
164 Climatology Project (GPCP) were used (Huffman, 2001). GPCP is a product derived
165 from observed rainfall data and precipitation estimates by geostationary and polar-
166 orbiting satellites. The spatial resolution of GPCP is $1^\circ \times 1^\circ$ degrees in latitude and
167 longitude. Additionally, estimates of Outgoing Longwave Radiation (OLR) from
168 National Oceanic and Atmospheric Administration (NOAA), with a spatial resolution of
169 $2.5^\circ \times 2.5^\circ$ degrees in latitude and longitude, were used for assessing the model ability
170 to represent the MJO in conjunction with zonal wind at 850 and 200 hPa from ERA-
171 Interim. This OLR estimation is generated through interpolations in time of polar-
172 orbiting satellite data (for additional information, see Liebmann and Smith, 1996).

173 Six BAM-1.2 configurations for sub-seasonal prediction have been defined for
174 evaluation. Characteristics such as vertical resolution, convection and boundary layer
175 parameterizations were evaluated as well as the impact of soil moisture initialization.
176 Single member hindcasts over the 1999/2000 – 2010/2011 extended austral summer
177 period were produced for each configuration. Five of the configurations were defined by
178 combining two convection schemes, the revised simplified Arakawa Shubert and the
179 modified Grell-Dévényi, and two vertical diffusion schemes for the PBL, the moist-PBL
180 Bretherton-Park scheme and the dry-PBL modified Mellor-Yamada, and two vertical
181 resolutions, 42 and 64 sigma levels. These physical processes and vertical resolutions of

182 the model were selected because they have an important influence on the predictive
183 ability of the MJO (Vitart, 2014; Boyle et al., 2015; Wang and Chen, 2017) and
184 consequently in the sub-seasonal precipitation and T2M predictions. It is important to
185 highlight that other aspects such as horizontal resolution, radiation and microphysics
186 parameterizations are also important for the good representation of the MJO (Zhang,
187 2005; Vitart, 2014; Wang et al., 2018). However, such characteristics were not
188 evaluated in the present work.

189 The sixth configuration evaluates the impact of soil moisture. This characteristic is a
190 source of predictability for the sub-seasonal timescale and has a positive impact on
191 GCM predictive ability, especially in longer lead times such as when predicting weeks 3
192 and 4 (Koster et al., 2010). In this part of the study, the mean soil moisture from the
193 previous month of the start date of each hindcast from the Global Land Data
194 Assimilation System (GLDAS) version 2 product (Rui and Beaudoin, 2017) was used
195 to initialize the soil moisture rather than using the monthly climatological soil moisture
196 estimate in order to assess whether a more realistic soil moisture condition has an
197 impact on the predictive ability of BAM-1.2. The monthly climatological soil moisture
198 data estimates used in this study were obtained from the balance analyses of Willmott et
199 al. (1985). Both GLDAS and climatological soil moisture data estimates were
200 interpolated to the model Gaussian grid and converted to soil moisture fraction for
201 hindcasts initialization.

202 The six examined configurations are defined in Table 2 and are summarized below:

- 203 • 42ABC: BAM-1.2 with 42 vertical levels, revised simplified Arakawa-Schubert
204 deep convection parameterization, moist Bretherton-Park boundary layer
205 parameterization, and climatological soil moisture initialization;
- 206 • 64ABC: BAM-1.2 with 64 vertical levels, revised simplified Arakawa-Schubert
207 deep convection parameterization, moist Bretherton-Park boundary layer
208 parameterization, and climatological soil moisture initialization;
- 209 • 42ABG: BAM-1.2 with 42 vertical levels, revised simplified Arakawa-Schubert
210 deep convection parameterization, moist Bretherton-Park boundary layer
211 parameterization, and soil moisture initialized through the GLDAS version 2
212 product;
- 213 • 42GBC: BAM-1.2 with 42 vertical levels, modified Grell-Dévényi deep
214 convection parameterization, moist Bretherton-Park boundary layer
215 parameterization, and climatological soil moisture initialization;
- 216 • 64GBC: BAM-1.2 with 64 vertical levels, modified Grell-Dévényi deep
217 convection parameterization, moist Bretherton-Park boundary layer
218 parameterization, and climatological soil moisture initialization;
- 219 • 42AMC: BAM-1.2 with 42 vertical levels, revised simplified Arakawa-Schubert
220 deep convection parameterization, dry modified Mellor-Yamada boundary layer
221 parameterization, and climatological soil moisture initialization.

222

223 2.3. Evaluation metrics and ensemble approaches

224 We assessed the ability of the six BAM-1.2 configurations to predict precipitation, T2M
225 and the MJO. For precipitation and T2M, the deterministic assessment consists of

226 computing the Pearson correlation and Root-Mean-Square Error (RMSE) between the
227 prediction and observed anomalies. Each metric was calculated for each grid point and
228 for four lead times: days 1-7 (week-1), 8-14 (week-2), 15-21 (week-3) and 22-28 (week-
229 4). The results were evaluated in the form of weekly averages because the model is
230 expected to have a greater ability to predict weekly anomalies than daily values when
231 producing sub-seasonal predictions (Vitart, 2014).

232 The performance of MJO prediction was evaluated using the Real-time Multivariate
233 MJO indices (RMMs) (Wheeler and Hendon, 2004). Reference RMMs were calculated
234 using the meridional wind at 850 and 200 hPa from the ERA-Interim reanalyses and
235 satellite observed OLR. RMMs for hindcasts were calculated as proposed by Rashid et
236 al. (2011). The metrics used for the MJO prediction quality assessment were bivariate
237 correlation and RMSE (Lin et al., 2008) with lead times in days.

238 In addition to the single member deterministic prediction assessment, we evaluated the
239 ability of the Multiple Configurations Ensemble (MCEN) mean prediction formed by
240 the six here investigated BAM-1.2 configurations with each configuration representing
241 one ensemble member. This was compared to an Initial Condition Ensemble (ICEN)
242 produced with an Empirical Orthogonal Function (EOF) perturbation methodology
243 (Mendonça and Bonatti, 2009), using the configuration that showed the best
244 performance among the six evaluated configurations for producing six ensemble
245 members. The EOF-based perturbation methodology is in operation at CPTEC for
246 extended range forecasts up to 15 days. The methodology produces optimally perturbed
247 analyses by applying the EOFs to n time series formed by the differences between a

248 model run initialized with a control initial condition and n model runs initialized with
249 randomly perturbed initial conditions. The initial random perturbations are drawn from
250 a Gaussian distribution with zero mean and standard deviation comparable to the model
251 short length forecast error [e.g., 3 ms^{-1} for the horizontal wind field components, 0.6 K
252 for the air temperature field, 1 hPa for the surface pressure field and a vertical standard
253 deviation profile for the specific humidity derived from the ECMWF background error
254 covariance matrix (Derber and Boutier, 1999)]. The EOF analysis is performed over the
255 Northern and Southern Hemispheres, over the tropical domain and also regionally over
256 southern and northern South America. The EOF perturbations are the ones associated
257 with the fast growth coefficients. To be used as optimal perturbations, these fast growth
258 modes are rescaled in order to have a standard deviation of the same order of magnitude
259 as the initial perturbations. Finally, the optimal perturbation is added and subtracted
260 to/from the control analysis and an ensemble of $2n$ initial perturbed states is produced.
261 A more detailed revision of the EOF-based perturbation methodology used at CPTEC
262 can be found in Cunningham et al. (2015).

263 The above mentioned deterministic metrics for precipitation and T2M anomaly
264 hindcasts, as well as for the hindcast MJO indices, were calculated for the ensemble
265 mean of the two equal size (six members) ensemble (MCEN and ICEN) to assess and
266 compare the value of utilizing multiple sub-seasonal predictions using two approaches.

267 In order to have an assessment of the differences in the obtained scores for the
268 investigated model configurations and the two ensemble mean approaches, 95%
269 confidence intervals were computed for the mean correlation and RMSE (for

270 precipitation and T2M anomalies), globally averaged between 60° N and 60° S, and for
271 the bivariate correlation and RMSE (for the MJO) using a bootstrap resampling
272 procedure with replacement with 1000 samples.

273 **3. HINDCAST QUALITY ASSESSMENT**

274 3.1. Deterministic evaluation of the six investigated BAM-1.2 configurations

275 Figure 1 shows the correlation between predicted and observed (GPCP) precipitation
276 anomalies for the six BAM-1.2 configurations (first 6 rows) and four lead times (four
277 columns representing week-1, week-2, week-3 and week-4). The 10 hindcasts per
278 extended austral summer (5 months times 2 start dates) over 12 austral summers
279 produce a sample with a total of 120 hindcasts. Applying a two-side Student's t test, the
280 correlation value of 0.2 is statistically significant, different from zero at the 5% level.

281 For the six configurations, in general, the correlation is high during the first week in
282 most regions and drops rapidly as lead time increases. This fall is more pronounced
283 between the first and second week for all six configurations as the forecasts extend
284 beyond the deterministic limit of predictability for many scales and we are considering
285 only a single member for this initial analysis. It is noted that all configurations show
286 greater correlation over the North Hemisphere than the South Hemisphere during week-
287 1 and week-2. This is because GCMs are more likely to predict winter baroclinic
288 weather systems and associated fronts (Zhu et al., 2014). As of the third week, BAM-
289 1.2 correlation values are smaller than 0.2 in practically all extratropical regions. This
290 illustrates that the predictive ability of BAM-1.2 over mid-latitudes beyond 15 days is
291 limited for single member hindcasts. For weeks 3 and 4, significant correlation values

292 are only seen in the Tropical Pacific Ocean, over a few areas in northern South America
293 and in the equatorial Atlantic Ocean. The high correlation values in the first two lead
294 times, especially at week-1, are associated to the predictability provided by the initial
295 conditions, and the high correlation values observed in the last two lead times over the
296 equatorial Pacific Ocean are mainly associated to the predictability provided by the El
297 Nino-Southern Oscillation (ENSO) and the MJO (Li and Robertson, 2015; de Andrade
298 et al., 2019). All six configurations show negligible correlation values near the
299 Subtropical Highs and desert regions from week-1. These characteristics are also
300 noticed in other GCMs configured for sub-seasonal predictions (Zhu et al, 2014; Li and
301 Robertson, 2015; Wheeler et al., 2017; de Andrade et al., 2019) and are associated with
302 the low capacity of GCMs to simulate small precipitation rates in these regions.

303 The spatial correlation pattern is similar for the four weeks of each of the six BAM-1.2
304 configurations. However, this pattern for the configurations with revised simplified
305 Arakawa-Schubert (deep convection) and moist Bretherton-Park (boundary layer)
306 parameterizations shows slightly larger values in the first two weeks than for the other
307 configurations (Figure 1, first two columns of configurations 42ABC, 64ABC and
308 42ABG vs. first two columns of configurations 42GBC, 64GBC and 42AMC). In the
309 week-3 and week-4 (last two columns of Figure 1), correlation levels are similar in
310 terms of both spatial pattern and intensity for the six configurations. Increasing the
311 vertical resolution shows very little change in the precipitation correlation levels at any
312 lead time. For example, the 42 vertical level configuration, 42ABC (first row of Figure
313 1), and the 64 vertical level configuration, 64ABC (second row of Figure 1), have
314 nearly identical correlation values for most regions. The same is noticed for

315 configurations 42GBC (fourth row of Figure 1) and 64GBC (fifth row of Figure 1).
316 Initialization of the soil moisture also shows no increase in the correlation values for all
317 four investigated weeks. Hindcasts initialised with climatological soil moisture
318 (42ABC, first row of Figure 1) have the same correlation levels as 42ABG (third row of
319 Figure 1) hindcasts, which were initialized with GLDAS soil moisture.

320 Figure 2 shows the precipitation anomaly RMSE spatial features for the six BAM-1.2
321 configurations. Highest RMSE values are found over the Intertropical Convergence
322 Zone (ITCZ), Indian Ocean, Maritime Continent, South Pacific Convergence Zone
323 (SPCZ) and South American Convergence Zone (SACZ), which are regions of strong
324 sub-seasonal variability (Liu et al., 2014). The errors grow as lead time increases. As for
325 the correlation assessment, the errors grow more between week-1 and week-2 than from
326 weeks 2 to 3. Again, configurations with revised simplified Arakawa-Shubert and moist
327 Bretherton-Park parameterizations have the fewest errors and do not differ greatly from
328 each other (rows 42ABC, 64ABC and 42ABG in Figure 2). Configurations with
329 modified Grell-Dévényi parameterizations (rows 42GBC and 64GBC in Figure 2) also
330 do not differ much from each other and have larger errors when compared to
331 configurations with revised simplified Arakawa-Shubert parameterizations. That is, the
332 revised simplified Arakawa-Shubert parameterization seems to be better than the
333 modified Grell-Dévényi parameterization and increase of the vertical resolution and soil
334 moisture initialization do not reduce the errors of the hindcasts in any lead time.

335 To better note the differences between the six configurations, the mean global
336 correlation between 60°N and 60°S was calculated as a function of lead time (Figure
337 3a). Vertical bars represent bootstrap 95% confidence intervals. The six configurations

338 show a near-exponential drop in correlation as a function of lead time. The
339 configurations with the revised simplified Arakawa-Shubert and moist Bretherton-Park
340 parameterizations (black, orange and blue lines) have the largest correlation values
341 when compared to the other configurations in the week-1 and week-2. Important
342 improvements are noticed when comparing the configurations with revised simplified
343 Arakawa-Shubert and modified Grell-Dévényi deep convection parameterizations at the
344 first two lead times. For example, 42ABC (black line) has a global mean correlation
345 equals to 0.45 at week-1 and drops to 0.18 at week-2, whereas 42GBC (yellow line) has
346 a global mean correlation values equals to 0.40 at week-1 and drops to 0.14 at week-2.
347 The 95% confidence intervals for the 42ABC (black vertical bars on top of solid black
348 line) do not overlap the 95% confidence intervals for the 42GBC (yellow vertical bars
349 on top of solid yellow line), illustrating the superiority of 42ABC over 42GBC.
350 However, the six configurations show similar correlation levels at week-4. As noted in
351 the previous figures, the increase of vertical resolution does not result in an increase in
352 the correlation values. This feature is noticed when we compare the 42ABC (black line)
353 and 64ABC (orange line) configurations or the 42GBC (yellow line) and 64GBC (green
354 line) configurations, which show practically the same behaviour, with the differences
355 between configurations smaller than the 95% confidence intervals (vertical bars). This is
356 also noticed for soil moisture initialization, where the 42ABG configuration (blue line)
357 shows similar correlation levels to the 42ABC configuration (black line).

358 The global RMSE mean between 60°N and 60°S (Figure 3b) further emphasizes the
359 differences between the revised simplified Arakawa-Shubert and modified Grell-
360 Dévényi deep convection parameterizations. The modified Grell-Dévényi

361 parameterization (green and yellow lines) produces larger errors than the revised
362 simplified Arakawa-Shubert parameterization (other lines) at all lead times. The
363 differences between the errors of these two parameterizations are much larger than the
364 95% confidence intervals (vertical bars) shown in Figure 3b, illustrating the superiority
365 of the revised simplified Arakawa-Shubert over the modified Grell-Dévényi
366 parameterization. The configurations 42ABC (black line) and 64ABC (orange line)
367 show very similar values at the four lead times, with overlapping 95% confidence
368 intervals. This is also noticed with the 42GBC (yellow line) and 64GBC (green line)
369 configurations. These results suggest that increasing the vertical resolution does not
370 decrease the RMSE. The initialization of soil moisture also does not contribute to the
371 reduction of error (black vs. blue lines). An interesting aspect is that the configuration
372 with dry modified Mellor-Yamada boundary layer parameterization (red line) has the
373 smallest error in the last two lead times.

374 Figure 4 shows the correlation between predicted and reanalyses (ERA-Interim) T2M
375 anomalies for the six configurations and four lead times. The six BAM-1.2
376 configurations show better prediction performance for T2M anomalies than
377 precipitation anomalies (see Figures 1 and 4). The correlation values decrease with lead
378 time. The highest correlation values are seen over cloud free oceanic regions (e.g.,
379 42ABC row in Figure 4). However, significant sub-seasonal correlation values exist
380 over a large portion of the global land domain. Over extratropical continental regions,
381 strong correlation values are observed in restricted regions at week 3 and 4, for
382 example, over the southeast of the United States and some regions over Asia. Over

383 tropical regions, correlation values are low in regions with high convective activity
384 (e.g., over the Maritime Continent).

385 The spatial correlation pattern is similar for the four weeks of the six BAM-1.2
386 configurations. The difference in performance between configurations with revised
387 simplified Arakawa-Shubert and modified Grell-Dévényi deep convection
388 parameterizations is not observed for T2M (e.g., row 42ABC vs. row 42GBC in Figure
389 4). Configurations with these two parameterizations have the same performance level
390 for the four weeks of lead time. There are differences when comparing the two
391 boundary layer parameterizations. The configuration with the dry modified Mellor-
392 Yamada parameterization (row 42AMC in Figure 4) shows reduced performance than
393 the other five configurations at all lead times, which were configured with the moist
394 Bretherton-Park boundary layer parameterization. Increasing vertical resolution from 42
395 (rows 42ABC and 42GBC in Figure 4) to 64 (rows 64ABC and 64GBC in Figure 4)
396 levels seems to slightly reduced prediction performance of extratropical T2M anomalies
397 in the first two weeks of lead times. Predictions with the initialisation of soil moisture
398 (row 42ABG in Figure 4) rather than the climatology soil moisture (row 42ABC in
399 Figure 4), show a slight improvement in correlation in the continental regions
400 (Australia, South and North Americas and Africa) at week 2 and 3 lead time.

401 Figure 5 shows the T2M anomaly RMSE spatial features for the six BAM-1.2
402 configurations. In all configurations, RMSE values grow with the lead time and are
403 generally lower over oceanic regions than over continental regions for all 4 lead times.
404 The highest RMSE values are noticed over Northern Hemisphere regions where there
405 are interactions between mid-latitude baroclinic system, and tropical convective

406 anomalies, which are usually associated with the MJO and circulation teleconnections
407 through Rossby waves (Stan et al., 2017; Hu et al., 2019). Over northern Asia, high
408 RMSE values are also noticed. The RMSE values are lower over the Southern
409 Hemisphere because there are fewer continental regions than over the Northern
410 Hemisphere, and baroclinic instability is lower at this time of the year in the Southern
411 Hemisphere. The latter makes the interaction between the convective anomalies over
412 tropical regions and circulation over mid-latitudes regions less pronounced. As a result,
413 the sub-seasonal variability over the Southern Hemisphere extratropical regions is also
414 reduced during the austral summer.

415 Configurations with the revised simplified Arakawa-Shubert and modified Grell-
416 Dévényi deep convection parameterizations present similar RMSE patterns (Figure 5).
417 Some differences are found in specific regions. For example, the 42GBC configuration
418 shows slightly lower RMSE values over southern South America than the 42ABC
419 configuration at week 3. The opposite is noticed over the Iberian Peninsula. Similar
420 features are noticed for the increase in vertical resolution. Concerning the initialization
421 of soil moisture, subtle differences are noticed between 42ABC and 42ABG, with slight
422 improvements over continental regions such as Australia, South America, southern
423 Africa and North America with initialized soil moisture (42ABG). Large differences are
424 found when comparing configurations with moist Bretherton-Park and dry modified
425 Mellor-Yamada boundary layer parameterizations. For example, the RMSE values are
426 lower in high latitude regions over North America and Asia for the 42AMC
427 configuration when compared to the 42ABC configuration. The opposite is over tropical
428 and medium latitudes regions.

429 Figure 6 shows the global mean T2M anomaly correlation (Figure 6a) and RMSE
430 (Figure 6b) averaged between 60°N and 60°S as a function of lead time with 95%
431 confidence intervals (vertical bars). The six configurations show a similar drop (rise) in
432 correlation (RMSE) as a function of lead time. The increase of vertical resolution from
433 42 to 64 levels, change of deep convection scheme and soil moisture initialization do
434 not influence the levels of correlation and error values for T2M anomalies predictions
435 for the global perspective. This feature is noticed by the proximity or overlap of
436 correlation and RMSE lines of most investigated configurations shown in Figure 6, with
437 overlapping 95% confidence intervals. Differences in performance levels are noticed
438 when comparing moist Bretherton-Park and dry modified Mellor-Yamada boundary
439 layer parameterizations. The dry modified Mellor-Yamada parameterization (red line)
440 produces smaller correlation values and larger errors than the other five configurations
441 at all lead times, with the differences between these configurations and the others larger
442 than the 95% confidence intervals (vertical bars) illustrating the superiority of the other
443 configurations.

444 Figures 7a and 7b show MJO bivariate correlation and bivariate RMSE of all six BAM-
445 1.2 configurations, respectively. Vertical bars represent bootstrap 95% confidence
446 intervals. The MJO predictive ability is determined when the bivariate correlation is
447 lower than 0.5 and the bivariate RMSE grows to $\sqrt{2}$. The lead times for these two
448 thresholds to be reached are usually found to be close (Rashid et al., 2011). The
449 bivariate correlation decreases with the increase in lead time and crosses the threshold
450 of 0.5 in 18-19 days for all configurations, except for the 42AMC configuration (red
451 line), which uses the dry modified Mellor-Yamada boundary layer parameterization and

452 has a much reduced performance, with the bivariate correlation reaching the 0.5
453 threshold in 12 days. The bivariate RMSEs (Figure 7b) increase with lead time and each
454 configuration reaches the bivariate RMSE value of $\sqrt{2}$ at approximately the same lead
455 time as the bivariate correlation. The 42AMC configuration crosses the threshold value
456 of $\sqrt{2}$ in 11 days, whereas the other five configurations cross the threshold value of $\sqrt{2}$
457 in around 18 to 19 days. The overlap of the 95% confidence intervals (vertical bars) for
458 most configurations (except 42AMC) illustrates their similarity in MJO predictive
459 ability.

460 3.2.Deterministic assessment of two investigated ensemble approaches

461 With the precipitation anomalies, T2M anomalies and MJO hindcast evaluation of the
462 six configurations shown in the previous section, a preferred BAM-1.2 configuration
463 was determined for defining an ensemble sub-seasonal forecasting system for CPTEC.
464 The increase of the vertical resolution from 42 levels to 64 levels did not result in
465 increase in predictive ability, therefore a vertical resolution of 42 levels was selected.
466 The moist Bretherton-Park boundary layer parameterization was selected because it
467 contributed to a better performance than the dry modified Mellor-Yamada boundary
468 layer parameterization, especially for T2M anomalies and MJO predictions. The revised
469 simplified Arakawa-Shubert and modified Grell-Dévényi deep convection
470 parameterizations showed similar ability for T2M anomalies and MJO prediction with a
471 slight advantage to the modified Grell-Dévényi parameterization for MJO prediction.
472 On the other hand, the revised simplified Arakawa-Shubert parameterization showed a
473 large advantage for sub-seasonal precipitation, with higher correlation and smaller
474 errors values than the modified Grell-Dévényi parameterization. Based on this

475 assessment, the revised simplified Arakawa-Shubert deep convection parameterization
476 was chosen. Soil moisture initialization instead of the climatology led to subtle
477 improvements in T2M anomalies predictions in specific regions (e.g., Australia).
478 However, these improvements were lower than expected and given limitations in the
479 availability of accurate real-time soil moisture data, the use of climatological soil
480 moisture was selected for the BAM-1.2 system. Therefore, the chosen BAM-1.2 version
481 for ensemble sub-seasonal forecasting was the 42ABC configuration.

482 The possible physical reasons why the selected configuration (42ABC) performed better
483 than the other investigated configurations, particularly in terms of the tested boundary
484 layer and deep convections parameterizations are as follows. The use of the moist
485 Bretherton-Park boundary layer parameterization resulted in better MJO and T2M
486 predictions performance than the use of the dry modified Mellor-Yamada boundary
487 layer parameterization. This is because the moist Bretherton-Park has several
488 advantages compared to the dry modified Mellor-Yamada parameterization. The main
489 contribution of the moist Bretherton-Park parameterization is to improve the
490 representation of the stable night boundary layer, where the predominant physical
491 process in flat areas such as the oceans is the surface radiative cooling. The evolution of
492 the stable nocturnal boundary layer depends on the radiative cooling rate, and therefore
493 the presence of clouds is essential for reducing radiative loss. At sunrise, the state of the
494 stable boundary layer will be important for the evolution of vertical instability and the
495 mixing boundary layer. Therefore, the higher or lower the energy released during the
496 evolution of the stable boundary layer this energy surplus or deficit will contribute to
497 the formation of shallow and deep clouds, and consequently impacts the daytime

498 temperature and precipitation cycle. The energy scales produced by these processes
499 directly or indirectly impact the atmospheric conditions on the sub-seasonal time scale.
500 As for the comparative performance of sub-seasonal precipitation predictions, important
501 differences were noted when changing the deep convection parameterizations. The
502 revised simplified Arakawa-Shubert parameterization showed better performance than
503 the modified Grell-Dévényi parameterization. This is likely due to the revision made by
504 Han and Pan (2011) in the simplified Arakawa-Shubert parameterization to suppress
505 unrealistic grid point storms due to remaining instability in the atmospheric column. We
506 next further assess BAM-1.2 sub-seasonal hindcast quality through a deterministic
507 evaluation of ensemble mean predictions. Two ensemble types are evaluated and
508 presented here. The first ensemble consists of one ensemble member from each of the
509 six configurations previously presented, which was denominated Multiple
510 Configurations Ensemble (MCEN). The second ensemble was denominated Initial
511 Condition Ensemble (ICEN) and is composed of six members produced with the chosen
512 42ABC configuration consisting of a control member and five perturbed members
513 produced with an EOF method (Mendonça and Bonatti, 2009; Cunningham et al.,
514 2015).

515 The assessment of the ensemble mean of the two ensemble types (MCEN and ICEN)
516 revealed important increase in global mean performance at four lead times for
517 precipitation anomalies predictions when compared to the single member assessment of
518 the six investigated BAM-1.2 configurations (Figure 3), with the increase in
519 performance larger than the 95% confidence intervals (vertical bars). The two ensemble
520 mean approaches show similar correlation levels (dashed lines in Figure 3a) and

521 overlapping 95% confidence intervals (vertical grey and black bars on top of dashed
522 lines). This shows that BAM-1.2 performance increases when more (six) members are
523 used to form an ensemble with the 42ABC configuration or when using the six
524 configurations as an ensemble. The predictive ability of GCMs increases as the number
525 of members increases because the ensemble mean acts as a filter for decreasing the
526 uncertainties of the initial conditions used to run the model (Cheung, 2001). This is
527 noticed over several regions in the four investigated lead times (e.g., Figure 1). For
528 example, over extratropical regions at week 2, over eastern South America at week 3
529 and over northern South America at week 4. Precipitation anomaly hindcasts also show
530 lower RMSE values for both ICEN and MCEN at all four lead times (dashed lines in
531 Figure 3b), with the reduction of error much larger than the 95% confidence intervals
532 (vertical bars). Improvements are noticed primarily over the ITCZ, Indian Ocean,
533 Maritime Continent, SPCZ and SACZ regions (last two rows in Figure 2). This suggests
534 that the ensemble mean helps BAM-1.2 to better represent the sub-seasonal variability
535 in these regions. The same feature is noticed for the T2M hindcasts ensemble means.
536 The two ensemble means show improved T2M anomalies performance when compared
537 to the single member performance with increased correlation values and decreased error
538 (see last two rows in Figure 4 and 5 and dashed lines in Figures 6). Improvements in
539 MJO forecast performance are also noticed when using the two ensemble approaches.
540 The prediction ability limits are around lead times 18 and 19 days for the single member
541 configurations, except for the 42AMC which is much reduced (solid lines in Figures 7).
542 For the MCEN this limit increases to 21 days (dashed grey line in Figures 7a-b) and to
543 20 days (dashed black line in Figures 7a-b) for the ICEN. However, these improvements

544 are less prominent than those identified for precipitation and T2M, because the 95%
545 confidence intervals of the two ensemble approaches largely encompass the 95%
546 confidence intervals of the single members of the individual investigated configurations.

547 **4. CONCLUSIONS**

548 Vertical resolution and physical parameterizations (deep convection and boundary
549 layer) were changed in BAM-1.2 to form five model configurations to determine the
550 model configuration with greater performance for sub-seasonal predictions. These
551 components were selected because these parameters have an important impact on
552 GCMs simulated MJO (Zhang, 2005; Wang and Chen, 2017; Wang et al., 2018). Given
553 the soil moisture initialization potential to increase the sub-seasonal predictions
554 performance (Koster et al., 2010; Koster et al., 2011; Guo et al., 2012), a further
555 configuration initialized with monthly soil moisture from the previous month, rather
556 than the climatological mean soil moisture, was formed to investigate the impact of soil
557 moisture initialization on BAM-1.2 predictive ability. The configuration with the best
558 result was selected to form an initial condition ensemble (ICEN) with six members, one
559 control member and five perturbed members produced using an EOF-based
560 methodology. The six configurations, individually evaluated in the first part of this
561 work, were also used to form another ensemble (multiple configurations ensemble-
562 MCEN) to compare the improvements inherent in the ensemble mean between ICEN
563 and MCEN.

564 All six BAM-1.2 configurations produced high precipitation and T2M anomalies
565 correlation levels for the first week and decreased correlation levels for weeks 2-4. For
566 weeks 3-4, moderate precipitation anomaly correlation levels were restricted to the

567 Equatorial Pacific Ocean region. This feature was also noticed in other models (e.g., Li
568 and Robertson, 2015; de Andrade et al., 2019). Precipitation anomaly RMSE increased
569 with lead time and the highest RMSE values were found over regions with strong sub-
570 seasonal variability, for example, over the ITCZ, Indian Ocean, Maritime Continent,
571 SPCZ and SACZ (Liu et al., 2013). For T2M, this characteristic was identified over the
572 Northern Hemisphere where interaction between anomalous convection and mid-
573 latitudes circulation anomalies are noticed (Hu et al., 2019). The six BAM-1.2
574 configurations showed better prediction performance for T2M anomalies than for
575 precipitation anomalies.

576 The increase of the vertical resolution from 42 levels to 64 levels did not result in an
577 increase in predictive ability. Comparing 42ABC with 64ABC (revised simplified
578 Arakawa-Shubert deep convection configurations with 42 and 64 levels, respectively)
579 and 42GBC with 64GBC (modified Grell-Dévényi deep convection configurations with
580 42 and 64 levels, respectively), it was noticed that the correlation and RMSE showed
581 nearly identical levels for all lead times for precipitation anomalies, T2M anomalies and
582 MJO predictions. These results may sound contradictory since other studies have shown
583 that the increase in vertical resolution contributes to improvements in predictive ability
584 in the sub-seasonal timescale (Zhang, 2005; Vitart, 2014). Other factors might be
585 contributing to this finding. For example, the use of initial conditions with only 37
586 vertical levels, which had to be interpolated to cover 42 and 64 levels.

587 BAM-1.2 configurations with revised simplified Arakawa-Shubert deep convection
588 parameterization showed better performance than BAM-1.2 configurations with
589 modified Grell-Dévényi deep convection parameterization for sub-seasonal

590 precipitation prediction, with the largest correlation levels found in the first two weeks
591 and the smallest RMSE in the four lead times. However, these two parameterizations
592 showed practically the same performance for T2M anomalies and MJO, with the
593 commonly used performance thresholds reached at 18/19 days of lead time. The fact
594 that the BAM-1.2 model presents increased ability for sub-seasonal precipitation
595 forecast with the revised simplified Arakawa-Shubert deep convection parameterization
596 compared to modified Grell-Dévényi and very similar ability for T2M and MJO is
597 intriguing. Han and Pan (2011) provided a revision of the simplified Arakawa-Shubert
598 deep convection in the National Centers for Environmental Prediction's (NCEP) global
599 forecast system. This revision aimed to suppress unrealistic gridpoint storms due to
600 remaining instability in the atmospheric column. This might be a possible reason for the
601 better BAM-1.2 performance in sub-seasonal precipitation anomaly forecasting with
602 revised simplified Arakawa-Shubert deep convection parameterization.

603 The moist Bretherton-Park boundary layer parameterization produced better
604 performance for precipitation anomalies, T2M anomalies and MJO predictions than the
605 dry modified Mellor-Yamada boundary layer parameterization. The greatest differences
606 were noticed for MJO predictions, where the bivariate correlation decreased more
607 sharply as a function of lead time with the configuration using the dry modified Mellor-
608 Yamada parameterization (42AMC) than for the other configurations. For this, the
609 42AMC has correlation below 0.5 and RMSE above $\sqrt{2}$ around the 11th day of lead
610 time. Large discrepancies were also noticed for T2M anomalies predictions when
611 comparing 42AMC with the other configurations.

612 We did not find important impacts of soil moisture initialization when compared to
613 climatological initialization on the predictive ability of precipitation anomalies in the
614 four investigated lead times. Slight improvements were seen for T2M anomaly
615 predictions in some continental regions. These improvements were smaller than those
616 found in Koster et al. (2010), Koster et al. (2011), Guo et al. (2012) and Van den Hurk
617 and et al. (2012), and might be related to differences in the investigated seasons, time
618 window, experiments or/and even to low BAM-1.2 sensitivity to soil moisture
619 initialization.

620 With the evaluation of the six configurations, it was possible to determine a
621 configuration for use as CPTEC sub-seasonal ensemble system. For this, the determined
622 configuration was the 42ABC. This configuration consists of a model version at TQ126
623 spatial resolution, 42 vertical sigma levels, revised simplified Arakawa-Shubert deep
624 convection parameterization, moist Bretherton-Park boundary layer scheme,
625 initialization with climatological soil moisture, CLIRAD-LW, CLIRAD-SW, Morrison
626 microphysics and the IBIS-2.6-CPTEC surface model.

627 The deterministic evaluation of ensembles (MCEN and ICEN), through the computation
628 of the ensemble means, presented considerable improvements when compared to the
629 single (control) member evaluation (42ABC). For precipitation and T2M anomalies
630 predictions, this improvement was noticed mainly in extratropical continental regions.
631 For MJO predictions, the ensemble means extended in two days the MJO prediction
632 ability limit (e.g., up to 20 days). It is interesting to note that the MCEN mean, formed
633 from the six configurations, showed very similar level of improvements to ICEN when
634 compared to the control member.

635 This work focused on determining a global CPTEC model configuration for sub-
636 seasonal prediction through a deterministic assessment using a limited number of
637 ensemble members (six). The results presented in this paper suggest that BAM-1.2 has
638 competitive performance to other S2S models (Vitart et al., 2017; Lim et al., 2018; de
639 Andrade et al. 2019). In a forthcoming paper, we plan to perform a probabilistic
640 assessment of the defined configuration with an increased number of ensemble
641 members and a more detailed comparison of BAM-1.2 with other S2S models. It is
642 worth mentioning that although the extended austral summer is a fundamental season
643 for Brazil (particularly in terms of precipitation) further work is needed in order to
644 evaluate the performance of the Brazilian model during other seasons for identifying
645 regions where best to trust the model for issuing operational sub-seasonal predictions.

646 **Acknowledgements**

647 We thank two anonymous reviewers for providing valuable comments and suggestions
648 that contributed for improving the quality of this manuscript. The first author was
649 supported by Conselho Nacional de Desenvolvimento Científico e Tecnológico (CNPq),
650 Coordenação de Aperfeiçoamento de Pessoal de Nível Superior (CAPES) and
651 University of Reading (ref GS18-179). CASC thanks CNPq, process 304586/2016-1,
652 and Fundação de Amparo à Pesquisa do Estado de São Paulo (FAPESP), process
653 2015/50687-8 (CLIMAX Project) for the support received. SJW was supported by
654 the National Centre for Atmospheric Science ODA national capability programme
655 ACREW (NE/R000034/1), which is supported by NERC and the GCRF. This research
656 was partially supported by the Climate Science for Services Partnership Brazil project

657 (CSSP-Brazil) funded by the Newton Fund. DCS was supported by CNPq (process

658 167804/2018-9).

659

660 **References**

- 661 Arakawa A and Schubert WH. 1974. Interaction of a cumulus cloud ensemble
- 662 Boyle JS, Klein SA, Lucas DD, Ma HY, Tannahill J and Xie S. 2015. The parametric
- 663 sensitivity of CAM5's MJO. *Journal of Geophysical Research: Atmospheres*. **120**:1424-
- 664 44.
- 665 Bretherton CS and Park S. 2009. A new moist turbulence parameterization in the
- 666 Community Atmosphere Model. *Journal of Climate*. **22**:3422-48.
- 667 Chen M, Wang W and Kumar A. 2010. Prediction of monthly-mean temperature: The
- 668 roles of atmospheric and land initial conditions and sea surface temperature. *Journal of*
- 669 *Climate*, **23**:717-725.
- 670 Cheung KK. 2001. A review of ensemble forecasting techniques with a focus on
- 671 tropical cyclone forecasting. *Meteorological Applications*. **8**:315-32.
- 672 Chou MD and Suarez, MJ. 1999. A solar radiation parameterization (CLIRAD-SW) for
- 673 atmospheric studies. NASA/TM-1999-104606, M. J. Suarez, Ed., Series on Global
- 674 Modeling and Data Assimilation. **15**, 40 pp.
- 675 Chou MD, Suarez MJ, Liang XZ, Yan MM and Cote C. 2001. A thermal infrared
- 676 radiation parameterization for atmospheric studies. NASA/TM-2001-104606, Vol. 19.
- 677 Cunningham C, Bonatti JP and Ferreira M. 2015. Assessing improved CPTEC
- 678 probabilistic forecasts on medium-range timescale. *Meteorological Applications*. **22**:
- 679 378-384.

680 de Andrade, FM, Coelho, CA and Cavalcanti, IF. 2019. Global precipitation hindcast
681 quality assessment of the Subseasonal to Seasonal (S2S) prediction project models.
682 *Climate Dynamics*, **52**: 5451-5475.

683 Dee DP, Uppala SM, Simmons AJ, Berrisford P, Poli P, Kobayashi S, Andrae U,
684 Balmaseda MA, Balsamo G, Bauer DP and Bechtold P. 2011. The ERA-Interim
685 reanalysis: Configuration and performance of the data assimilation system. *Quarterly*
686 *Journal of the royal meteorological society*. **137**:553-97.

687 Derber J and Bouttier F. 1999. A reformulation of the background error covariance in
688 the ECMWF global data assimilation system. *Tellus A: Dynamic Meteorology and*
689 *Oceanography*. **51**: 195-221.

690 Figueroa SN, Bonatti JP, Kubota PY, Grell GA, Morrison H, Barros SR, Fernandez JP,
691 Ramirez E, Siqueira L, Luzia G and Silva J. 2016. The Brazilian global atmospheric
692 model (BAM): performance for tropical rainfall forecasting and sensitivity to
693 convective scheme and horizontal resolution. *Weather and Forecasting*, **31**: 1547-1572.

694 Green BW, Sun S, Bleck R, Benjamin SG and Grell GA. 2017. Evaluation of MJO
695 predictive skill in multiphysics and multimodel global ensembles. *Monthly Weather*
696 *Review*. **145**: 2555-2574.

697 Grell GA and Freitas SR. 2014: A scale and aerosol aware stochastic convective
698 parameterization for weather and air quality modeling. *Atmos. Chem. Phys.*, **14**: 5233–
699 5250.

700 Grell GA. 1993. Prognostic evaluation of assumptions used by cumulus
701 parameterizations. *Mon. Wea. Rev.* **121**: 764–787.

702 Grell, GA and Dévényi D. 2002. A generalized approach to parameterizing convection
703 combining ensemble and data assimilation techniques. *Geophysical Research Letters*,
704 29: 38-1.

705 Guo Z, Dirmeyer PA, DelSole T and Koster RD. 2012. Rebound in atmospheric
706 predictability and the role of the land surface. *Journal of Climate*. **25**: 4744-9.

707 Han J and Pan HL. 2011. Revision of convection and vertical diffusion schemes in the
708 NCEP global forecast system. *Weather and Forecasting*. **26**: 520-33.

709 Hu W, Liu P, Zhang Q and He B. 2019. Dominant patterns of winter-time intraseasonal
710 surface air temperature over the CONUS in response to MJO convections. *Climate*
711 *Dynamics*. 1-20.

712 Hudson D, Alves O, Hendon HH and Marshall AG. 2011. Bridging the gap between
713 weather and seasonal forecasting: intraseasonal forecasting for Australia. *Quarterly*
714 *Journal of the Royal Meteorological Society*, **137**: 673-689.

715 Huffman GJ, Adler RF, Morrissey MM, Bolvin DT, Curtis S, Joyce R, McGavock B
716 and Susskind J. 2001. Global precipitation at one-degree daily resolution from
717 multisatellite observations. *Journal of hydrometeorology*. **2**:36-50.

718 Koster RD, Mahanama SP, Yamada TJ, Balsamo G, Berg AA, Boisserie M, Dirmeyer
719 PA, Doblus-Reyes FJ, Drewitt G, Gordon CT, Guo Z. 2010. Contribution of land
720 surface initialization to subseasonal forecast skill: First results from a multi-model
721 experiment. *Geophysical Research Letters*. **37**.

722 Koster RD, Mahanama SP, Yamada TJ, Balsamo G, Berg AA, Boisserie M, Dirmeyer
723 PA, Doblas-Reyes FJ, Drewitt G, Gordon CT and Guo Z. 2011. The second phase of the
724 global land–atmosphere coupling experiment: soil moisture contributions to subseasonal
725 forecast skill. *Journal of Hydrometeorology*. **12**: 805-22.

726 Kubota PY. 2012. Variability of storage energy in the soil-canopy system and its impact
727 on the definition of precipitation standard in South America (in Portuguese with abstract
728 in English). Ph. D. thesis, Instituto Nacional de Pesquisas Espaciais (INPE), São José
729 dos Campos, Brazil.

730 Kumar A, Chen M and Wang W. 2011. An analysis of prediction skill of monthly mean
731 climate variability. *Climate dynamics*, **37**: 1119-1131.

732 Li S and Robertson AW. 2015. Evaluation of submonthly precipitation forecast skill
733 from global ensemble prediction systems. *Monthly Weather Review*, 143: 2871-2889.

734 Liang P and Lin H. 2018. Sub-seasonal prediction over East Asia during boreal summer
735 using the ECCO monthly forecasting system. *Climate dynamics*, **50**: 1007-1022.

736 Liebmann B and Smith CA. 1996. Description of a complete (interpolated) outgoing
737 longwave radiation dataset. *Bulletin of the American Meteorological Society*. **77**:1275-
738 7.

739 Lim Y, Son SW and Kim D. 2018. MJO prediction skill of the subseasonal-to-seasonal
740 prediction models. *Journal of Climate*, **31(10)**: 4075-4094.

741 Lin H, Brunet G and Derome J. 2008. Forecast skill of the Madden–Julian oscillation in
742 two Canadian atmospheric models. *Monthly Weather Review*. **136**: 4130-49.

743 Lin H, Gagnon N, Beaugregard S, Muncaster R, Markovic M, Denis B and Charron M.
744 2016. GEPS-based monthly prediction at the Canadian Meteorological Centre. Monthly
745 Weather Review, **144**: 4867-4883.

746 Liu X, Wu T, Yang S, Li T, Jie W, Zhang L, Wang Z, Liang X, Li Q, Cheng Y and Ren
747 H. 2017. MJO prediction using the sub-seasonal to seasonal forecast model of Beijing
748 Climate Center. Climate Dynamics, **48**: 3283-3307.

749 Liu X, Yang S, Li Q, Kumar A, Weaver S and Liu S. 2014. Subseasonal forecast skills
750 and biases of global summer monsoons in the NCEP Climate Forecast System version
751 2. Climate dynamics. **42**:1487-508.

752 Mastrangelo D, Malguzzi P, Rendina C, Drofa O and Buzzi A. 2012. First outcomes
753 from the CNR-ISAC monthly forecasting system. Advances in Science and Research,
754 **8**:77-82.

755 Mellor GL and Yamada T. 1982: Development of a turbulence closure model for
756 geophysical fluid problems. Rev. Geophys. Space Phys. **20**: 851–875

757 Mendonça AM and Bonatti J. 2009. Experiments with EOF-based perturbation methods
758 and their impact on the CPTEC/INPE ensemble prediction system. Monthly Weather
759 Review. **137**:1438-59.

760 Morrison H, Thompson G and Tatarskii V. 2009. Impact of cloud microphysics on the
761 development of trailing stratiform precipitation in a simulated squall line: Comparison
762 of one-and two-moment schemes. Monthly weather review. **137**: 991-1007.

763 Rashid HA, Hendon HH, Wheeler MC and Alves O. 2011. Prediction of the Madden–
764 Julian oscillation with the POAMA dynamical prediction system. *Climate Dynamics*.
765 **36**: 649-61.

766 Reichler T and Roads JO. 2005. Long-range predictability in the tropics. Part I: monthly
767 averages. *Journal of climate*, **18**: 619-633.

768 Rui H and Beaudoin H. 2017. Readme document for GLDAS Version 2 data products.
769 NASA Goddard Space Flight Center. **610**: 1-21.

770 Saha S, Moorthi S, Wu X, Wang J, Nadiga S, Tripp P, Behringer D, Hou YT, Chuang,
771 HY, Iredell M and Ek M. 2014. The NCEP climate forecast system version 2. *Journal of*
772 *Climate*. **27**: 2185-2208.

773 Shelly A, Xavier P, Copsey D, Johns T, Rodríguez JM, Milton S and Klingaman N.
774 2014. Coupled versus uncoupled hindcast simulations of the Madden-Julian Oscillation
775 in the Year of Tropical Convection. *Geophysical Research Letters*. **41**: 5670-7.

776 Stan C, Straus DM, Frederiksen JS, Lin H, Maloney ED and Schumacher C. 2017.
777 Review of tropical-extratropical teleconnections on intraseasonal time scales. *Reviews*
778 *of Geophysics*. **55**: 902-37.

779 Tarasova TA and Fomin BA. 2000. Solar radiation absorption due to water vapor:
780 Advanced broadband parameterizations. *Journal of Applied Meteorology*. **39**: 1947-
781 1951.

782 van den Hurk B, Doblas-Reyes F, Balsamo G, Koster RD, Seneviratne SI and Camargo
783 H. 2012. Soil moisture effects on seasonal temperature and precipitation forecast scores
784 in Europe. *Climate Dynamics*. **38**: 349-62.

785 Vitart F, Ardilouze C, Bonet A, Brookshaw A, Chen M, Codorean C, Déqué M, Ferranti
786 L, Fucile E, Fuentes M and Hendon H. 2017. The subseasonal to seasonal (S2S)
787 prediction project database. *Bulletin of the American Meteorological Society*. **98**: 163-
788 173.

789 Vitart F. 2004. Monthly forecasting at ECMWF. *Monthly Weather Review*, **132**: 2761-
790 2779.

791 Vitart F. 2014. Evolution of ECMWF sub-seasonal forecast skill scores. *Quarterly*
792 *Journal of the Royal Meteorological Society*. **140**: 1889-1899.

793 Vitart F. 2017. Madden—Julian oscillation prediction and teleconnections in the S2S
794 database. *Quarterly Journal of the Royal Meteorological Society*. **143**: 2210-2220.

795 Wang B and Chen G. 2017. A general theoretical framework for understanding essential
796 dynamics of Madden–Julian oscillation. *Climate Dynamics*. **49**: 2309-28.

797 Wang B, Lee SS, Waliser DE, Zhang C, Sobel A, Maloney E, Li T, Jiang X and Ha KJ.
798 2018. Dynamics-oriented diagnostics for the Madden–Julian Oscillation. *Journal of*
799 *Climate*. **31**: 3117-3135.

800 Weber, NJ and Mass, CF. 2017. Evaluating CFSv2 subseasonal forecast skill with an
801 emphasis on tropical convection. *Monthly Weather Review*, **145**: 3795-3815.

802 Wheeler MC and Hendon HH. 2004. An all-season real-time multivariate MJO index:
803 Development of an index for monitoring and prediction. *Monthly Weather Review*. **132**:
804 1917-32.

805 Wheeler MC, Zhu H, Sobel AH, Hudson D and Vitart F. 2017. Seamless precipitation
806 prediction skill comparison between two global models. *Quarterly Journal of the Royal*
807 *Meteorological Society*, **143**: 374-383.

808 Willmott CJ, Rowe CM and Mintz Y. 1985. Climatology of the terrestrial seasonal
809 water cycle. *International Journal of Climatology*. **5**: 589-606.

810 with the large-scale environment, Part I. *J. Atmos. Sci.* **31**: 674–701.

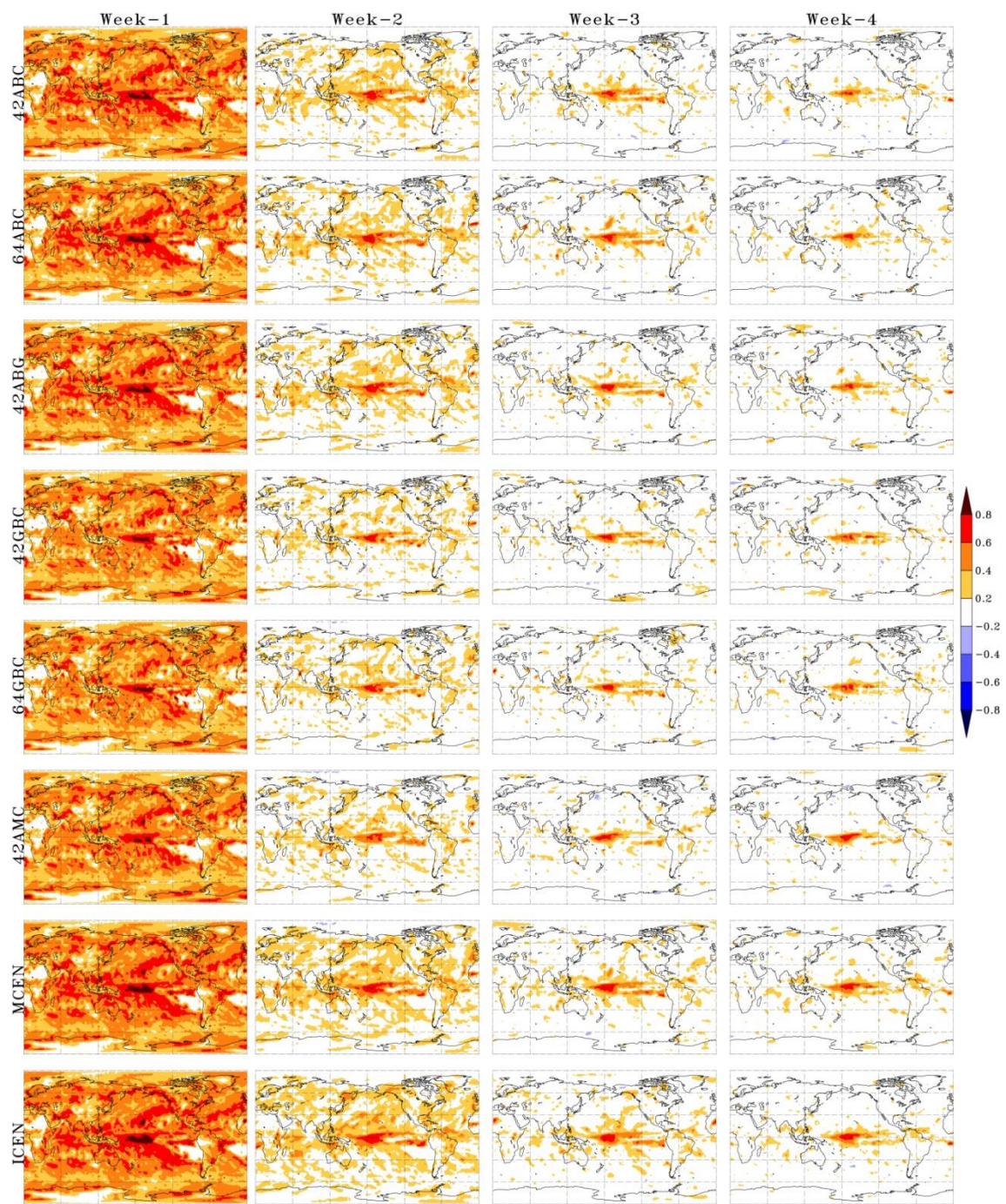
811 Yu H, Kaufman YJ, Chin M, Feingold G, Remer LA, Anderson TL, Balkanski Y,
812 Bellouin N, Boucher O, Christopher S and DeCola P. 2006. A review of measurement-
813 based assessments of the aerosol direct radiative effect and forcing. *Atmospheric*
814 *Chemistry and Physics*. **3**: 613-66.

815 Zhang C. 2005. Madden-Julian oscillation. *Reviews of Geophysics*. **43**.

816 Zhang C. 2013. Madden–Julian oscillation: Bridging weather and climate. *Bulletin of*
817 *the American Meteorological Society*. **94**: 1849-1870.

818 Zhu H, Wheeler MC, Sobel AH and Hudson D. 2014. Seamless precipitation prediction
819 skill in the tropics and extratropics from a global model. *Monthly Weather Review*, **142**:
820 1556-1569.

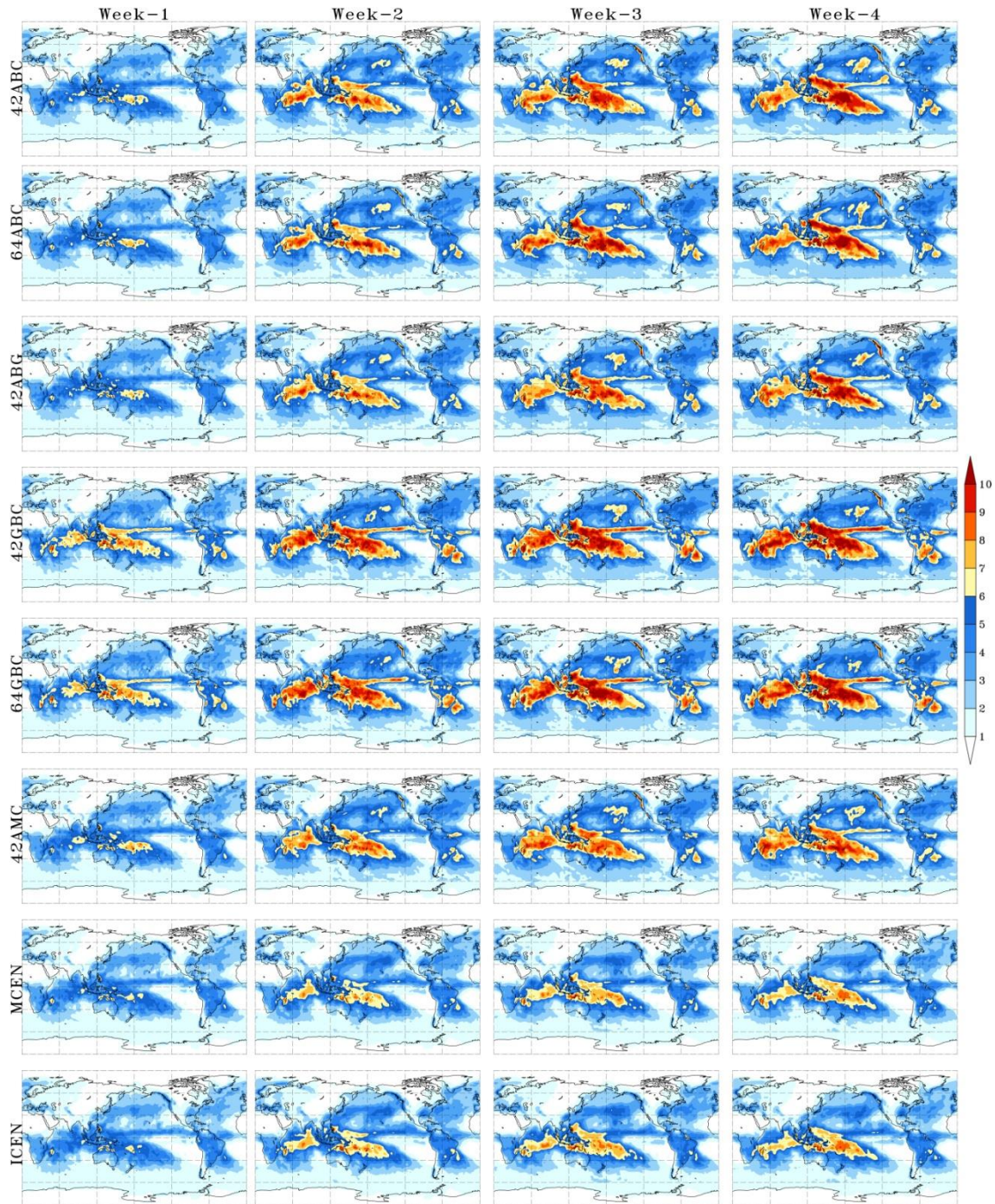
821



822

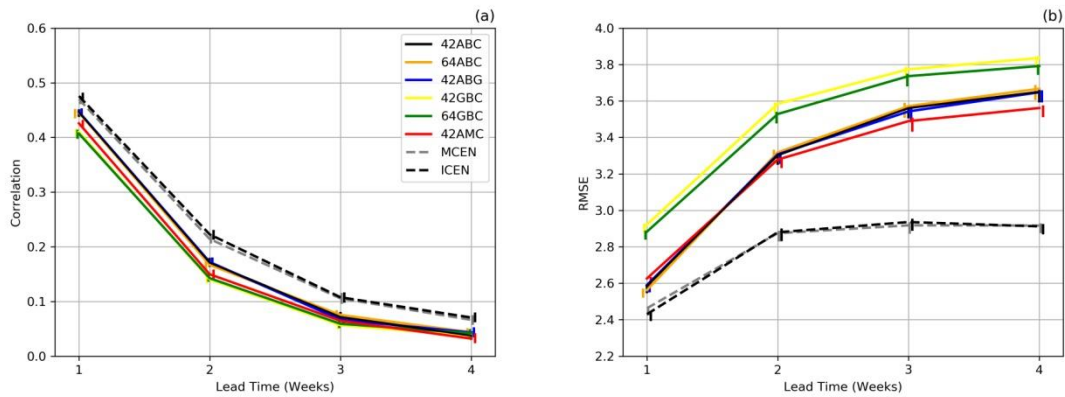
823 Figure 1: Correlation between the predicted and observed (GPCP) precipitation
 824 anomalies for the six BAM-1.2 configurations (42ABC, 64ABC, 42ABG, 42GBC,
 825 64GBC and 42AMC) and two ensemble means (MCEN and ICEN) (rows) for week-1,
 826 week-2, week-3 and week-4 (columns). The hindcasts were initialized within the

827 extended austral summer period (from November to March 1999/2000 – 2010/2011) on
828 the dates shown in Table 1.



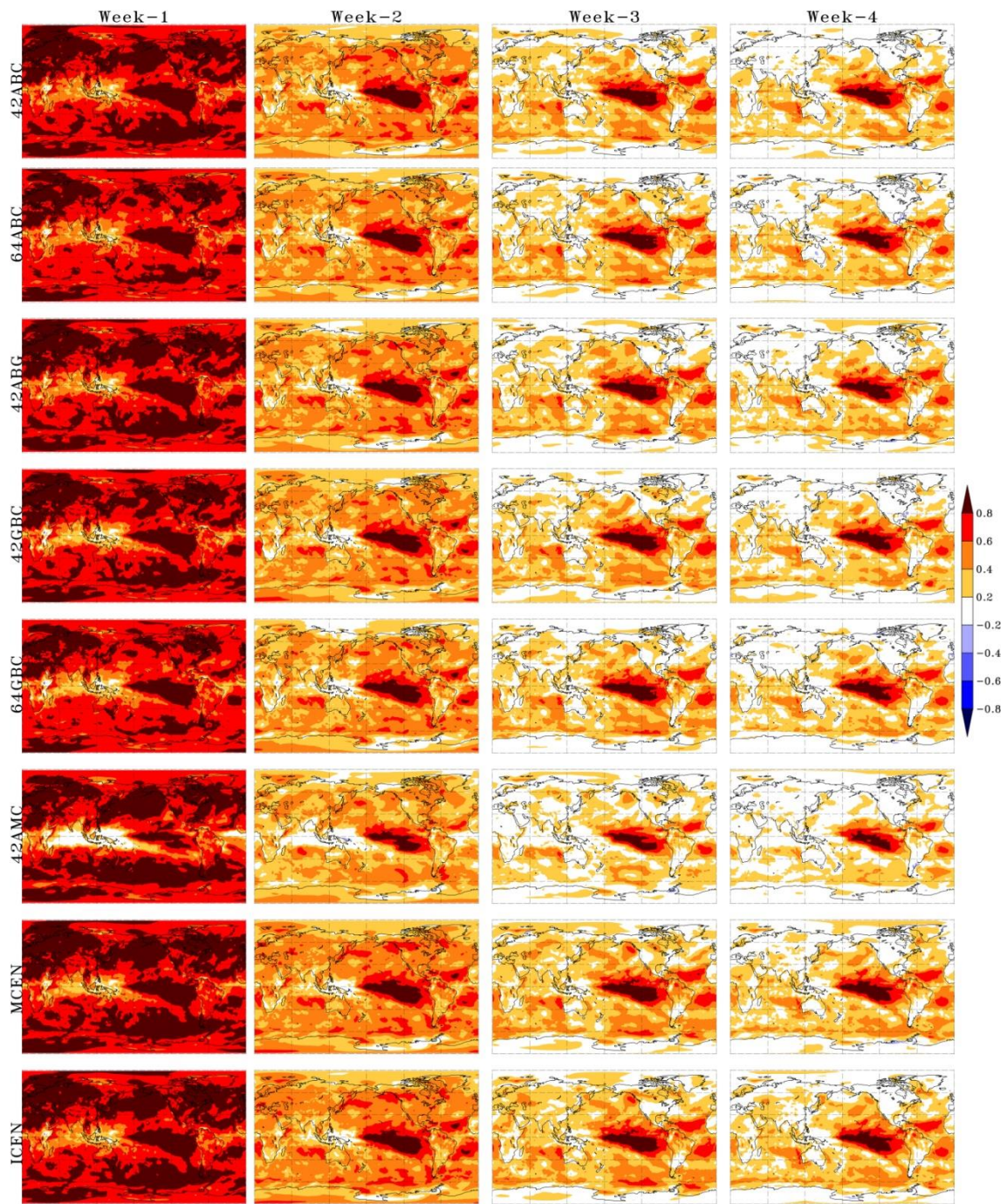
829
830 Figure 2: Six configurations (42ABC, 64ABC, 42ABG, 42GBC, 64GBC and 42AMC)
831 and two ensemble means (MCEN and ICEN) (rows) RMSE precipitation anomaly
832 (units are mm day⁻¹) for week-1, week-2, week-3 and week-4 (columns). The hindcasts

833 were initialized within the extended austral summer period (from November to March
 834 1999/2000 – 2010/2011) on the dates shown in Table 1.



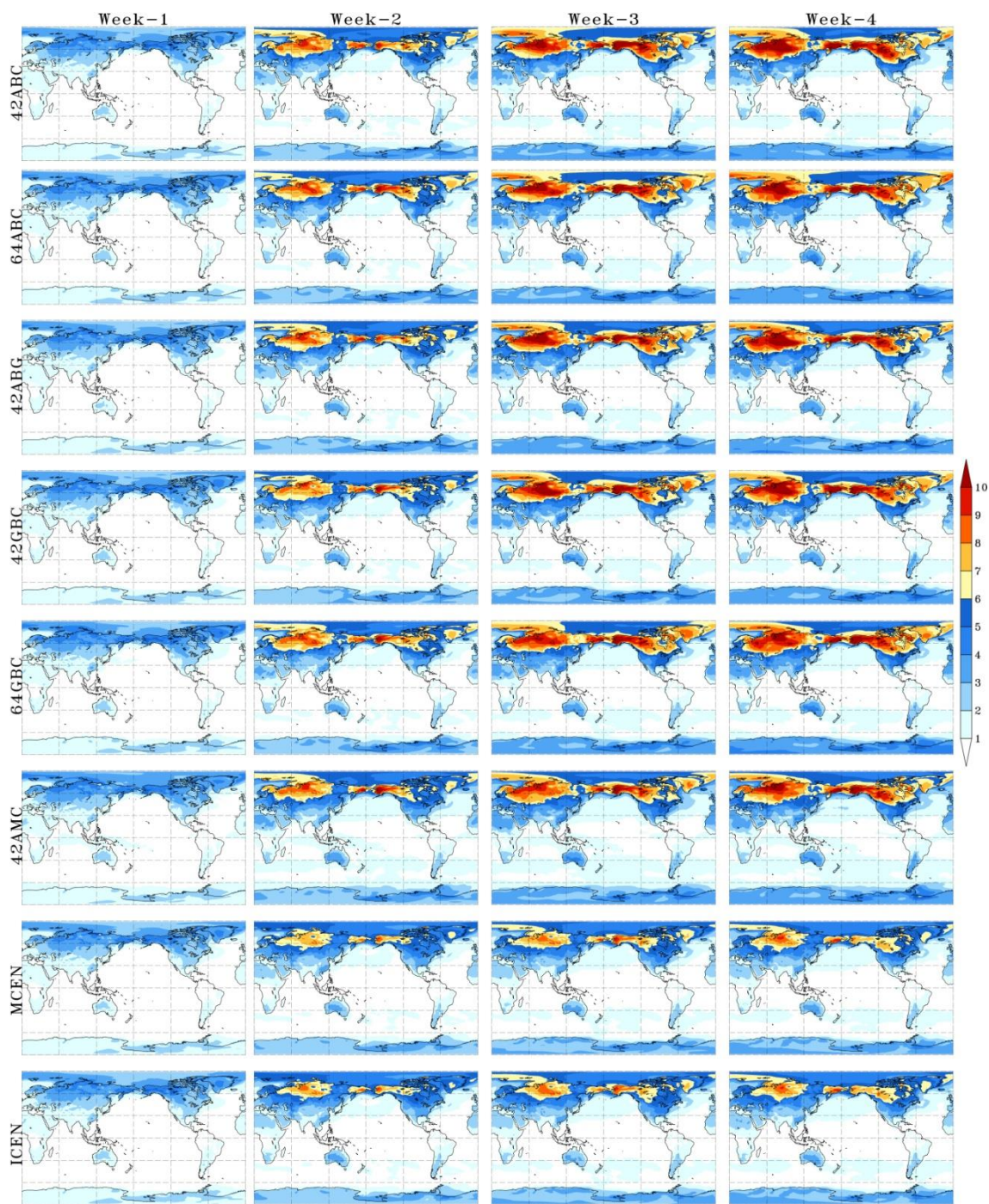
835

836 Figure 1: Global mean correlation between predicted and observed precipitation
 837 anomalies (a) and RMSE (b) for six BAM-1.2 configurations (42ABC, 64ABC,
 838 42ABG, 42GBC, 64GBC and 42AMC) and two ensemble approaches (MCEN and
 839 ICEN) assessed against GPCP averaged over the latitudinal band 60°N-60°S for four
 840 lead times (weeks 1 to 4). The hindcasts were initialized within the extended austral
 841 summer period (from November to March 1999/2000 – 2010/2011) on the dates shown
 842 in Table 1. The vertical bars plotted around the four lead times represent 95%
 843 confidence intervals produced using a bootstrap resampling procedure with replacement
 844 with 1000 samples. These vertical bars are slightly displaced from the exact lead time
 845 location in the horizontal axis to facilitate visualization.



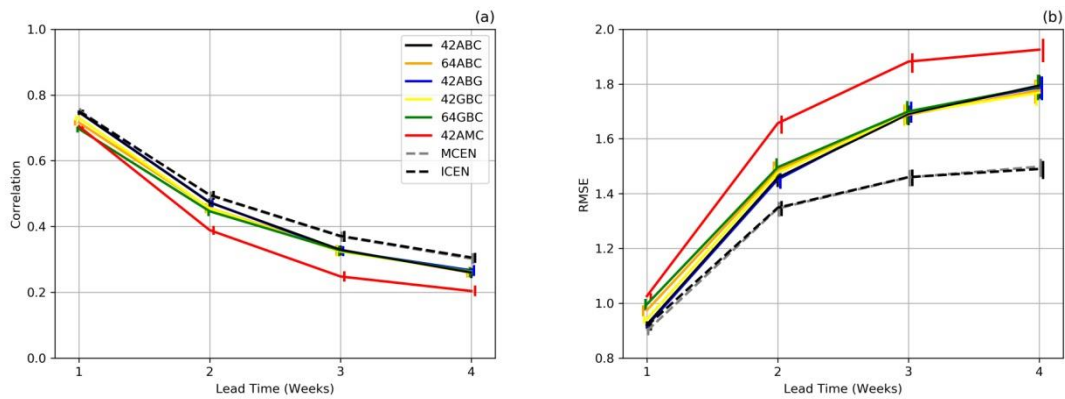
846

847 Figure 4: Same as Figure 1, except for T2M anomaly.



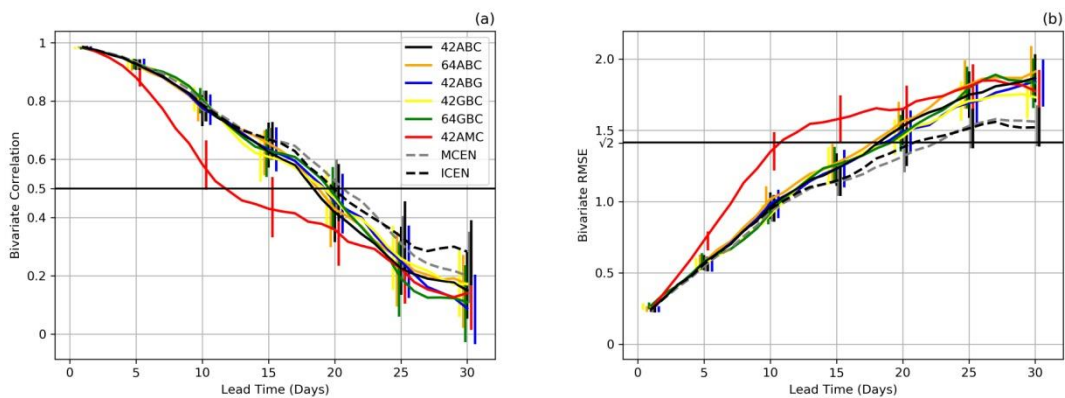
848

849 Figure 5: Same as Figure 2, except for T2M anomaly (units are °C).



850

851 Figure 6: Same as Figure 3, except for T2M anomaly.



852

853 Figure 2: Bivariate correlation (a) and bivariate RMSE (b) for six BAM-1.2 configurations
 854 (42ABC, 64ABC, 42ABG, 42GBC, 64GBC and 42AMC) and the two ensemble approaches
 855 (MCEN and ICEN) as a function of forecast lead time (in days). The hindcasts were initialized
 856 within the extended austral summer period (from November to March 1999/2000 – 2010/2011)
 857 on the dates shown in Table 1. The vertical bars around lead times 1 to 30 days plotted every 5
 858 days represent 95% confidence intervals produced using a bootstrap resampling procedure with
 859 replacement with 1000 samples. These vertical bars are slightly displaced from the exact lead
 860 time location in the horizontal axis to facilitate visualization. Note that two black vertical bars
 861 are plotted every 5 days, with the first of these bars corresponding to 42ABC and the second
 862 corresponding to ICEN.

863